Postprint of: Ullah U., Al-Hasan M., Kozieł S., Mabrouk I., A Series-Inclined-Slot-Fed Circularly Polarized Antenna for 5G 28-GHz Applications, IEEE Antennas and Wireless Propagation Letters (2021), pp.1-5, DOI: 10.1109/LAWP.2021.3049901

© 2021 IEEE. Personal use of this material is permitted. Permission from IEEE must be obtained for all other uses, in any current or future media, including reprinting/republishing this material for advertising or promotional purposes, creating new collective works, for resale or redistribution to servers or lists, or reuse of any copyrighted component of this work in other works.

This article has been accepted for publication in a future issue of this journal, but has not been fully edited. Content may change prior to final publication. Citation information: DOI 10.1109/LAWP.2021.3049901, IEEE Antennas and Wireless Propagation Letters

A Series-Inclined-Slot-Fed Circularly Polarized Antenna for 5G 28-GHz Applications

Ubaid Ullah, *Member, IEEE,* Muath Al-Hasan, *Senior Member, IEEE,* Slawomir Koziel, *Senior Member, IEEE,* and Ismail Ben Mabrouk, *Senior Member, IEEE*

***Abstract*—This letter presents the design of a single-point-fed, geometrically simple circularly polarized (CP) antenna for 28 GHz Ka-band applications. The proposed antenna is based on a straight microstrip line printed on one side and coupled with the nearly square patches through a 45-degree inclined V-shape slot aperture on the other side. In order to generate circular polarization, the fundamental radiating mode is degenerated at a slightly different frequency by aligning the patch edges parallel to each arm of the V-slot with orthogonal arms. This configuration yields a relatively small size (10 mm × 27.7 mm), wideband, and high-gain right-hand circularly polarized antenna operating at 28 GHz. The impedance bandwidth of the proposed antenna is from 27.2 GHz to 30.35 GHz and the 3 dB axial ratio (AR) bandwidth from 27.3 GHz to 29.7 GHz with excellent directional characteristics in the broadside direction. The peak gain is approximately 11.65 dBic. The performance characteristics in terms of the impedance matching, AR, gain and efficiency of the antenna for wearable applications are also investigated both numerically and experimentally. For practical applications, the small size of the structure allows for implementing the systems that consist of more than one antenna to account for user mobility.**

***Index Terms*— circularly polarized antenna, 5G, millimeter-wave antenna, EM-driven design.**

I. Introduction

In recent years, the demand for attaining high data rates in the range of gigabite per second, and scarce spectrum resources in currently utilized bands, has prompted the shift towards the millimeter-wave (mm-wave) band. The nascent 28 GHz band has attracted a serious attention, which been growing at an unprecedented rate since the intial roll-out of the 5th generation (5G) technology [1-3]. The extraordinatry high data rate handling capability of the mm-wave is due to the short communication wavelengths, larger frequency bandwidth and low signal interference. On the other hand, as a consequence of the Friis formula, the shortcoming of the mm-wave band is the path loss due to signal attenuation caused by varying atmospheric conditions [4-6]. The incorporation of the conventional linearly polarized antennas would significantly degrade the mm-wave performance due to the mismatch losses [7]. Following the rapid popularization of the 28 GHz 5G band among the industries and academia, the researchers have started investigating circularly polarized antennas for mm-wave applications. The mair reason is that circularly polarized waves are known to provide improved channel performance by alleviating the multipath interference, low absorption losses, and signal attenuation [8-11]. Moreover, mm-wave communication has the advantage of utilizing highly directive beams to combat the challenges of path losses and blockages. To further compensate for performance degradation, along with the polarization of the wave, gain enhancement of the antenna at the transmitting and the receiving end is required without additional power consumptions and implementation costs [12].

The various types of single-point-fed circularly polarized antennas have been designed for the 5G mm-wave bands [13-17]. In [13], a low profile single-layer mm-wave antenna with a modified ring shape is presented. The performance of the antenna in terms of the impedance bandwidth and the axial ratio bandwidth is excellent but the beam is very wide and tilted away from the broadside direction. Also, the gain of the antenna is roughly 6.5 dBic, which limits its application. Similarly, the designs presented in [14-17] involve a complex configuration of the radiator and the overall antenna structure hinders its practical implementations. To effectively exploit the potential of the mm-wave band, a high-gain phased array with directional beams is desired. Phased arrays are generally designed with either series or parallel feeding techniques. The complexity of the parallel feeding technique makes them less favorable due to the added circuit elements in the form of line discontinuities, power dividers, and phase shifters. These additional components of the feeding network not only increase the cost of the circuit but also add to the footprint ares of the antenna, which causes unwanted spurious radiation, dielectric losses and eventually reduces the antenna efficiency [18]. The cost effectiveness of the phased array can be achieved with the series feeding. A properly designed series-fed array can suppress the grating lobes and sidelobes, resulting in a lesser beam squint and higher gain.

Following the above discussion, in this letter, a one dimensional series-inclined slot-fed nearly square patch antenna is presented. The proposed antenna is based on the aperture coupled periodically placed slotted patches. A straight microstrip line is printed on one side of the substrate, and the open end of the feedline is terminated with a stub for impedance matching. Four V-shape slots are etched in the ground plane approximately half guided wavelength

Manuscript submitted on July …, 2020. This work was supported in part by the ADEK Award for Research Excellence (AARE19-245) 2019. the Icelandic Centre for Research (RANNIS) Grant 174114051, and by the National Science Centre of Poland Grant 2017/27/B/ST7/00563.

U.Ullah, and M. Al-Hasan are with Networks and Communication Engineering department, Al Ain university, P.O.Box (112612), Abu Dhabi, UAE. (ubaid.ullah@aau.ac.ae). Koziel is with Engineering Optimization and Modeling Center of Reykjavik University, Reykjavik, Iceland and also with the Faculty of Electronics, Telecommunications and Informatics, Gdansk University of Technology, 80-233 Gdansk, Poland (e-mail: koziel@ru.is). Ismail Mabrouk is with the engineering department, Durham University, Durham, United Kingdom (ismail.benmabrouk@durham.ac.uk).

1536-1225 (c) 2020 IEEE. Personal use is permitted, but republication/redistribution requires IEEE permission. See http://www.ieee.org/publications_standards/publications/rights/index.html for more information.
Authorized licensed use limited to: Reykjavik University. Downloaded on January 19,2021 at 12:47:27 UTC from IEEE Xplore. Restrictions apply.

This article has been accepted for publication in a future issue of this journal, but has not been fully edited. Content may change prior to final publication. Citation information: DOI 10.1109/LAWP.2021.3049901, IEEE Antennas and Wireless Propagation Letters

(corresponding to 28 GHz) away from each other. Four patches are printed on the same substrate as that of the feedline, and stacked above the slotted ground plane. The dimensions of the 45-degree inclined slot and the position of the patch edges with respect to the slot controls the excitation of orthogonal components for circular polarization. To ensure zero degree reflection phase and highly directional beams in the broadside direction, a metal layer is placed 1.5 mm below the feedline. The proposed design strategy allows for a relatively simple design due to a single feed. The antenna is easy to fabricate, exhibits high-gain and directive beams, both being desired attributes for 5G mm-wave applications. The design is evaluated numerically and fully optimized before fabrication, and validated experimentally in the free-space as well as on-body.

II. Single Port Series-Fed Antenna Design Configuration And Analysis

A. Antenna Design

The geometry of each layer of the proposed single point-fed series array antenna and its stacking configuration is illustrated in Fig. 1. All layers are printed on a thin laminated Rogers RO4003C substrate ($\varepsilon_r = 3.38$, $h = 0.508$ mm, $\tan\delta = 0.0027$), of external dimensions $l_s \times w_s$. The substrate widths are extended to w_s for connecting the port but the antenna can be realized with the width w_g. A 50-ohm straight microstrip line, terminated with an inclined stub at the open end, is used to excite the antenna. The reflector (Layer 1) is printed on a separate substrate whereas the feeding line (layer 2) and the slotted ground plane (Layer 3) are printed on the faces of a double-sided laminated substrate. As in general, highly-directional, high-gain antennas are desired for the mm-wave band, Layer 1 placed at a distance 'd' serves as a reflector. The radiating patches (Layer 4) are printed and stacked on the top of the slots.

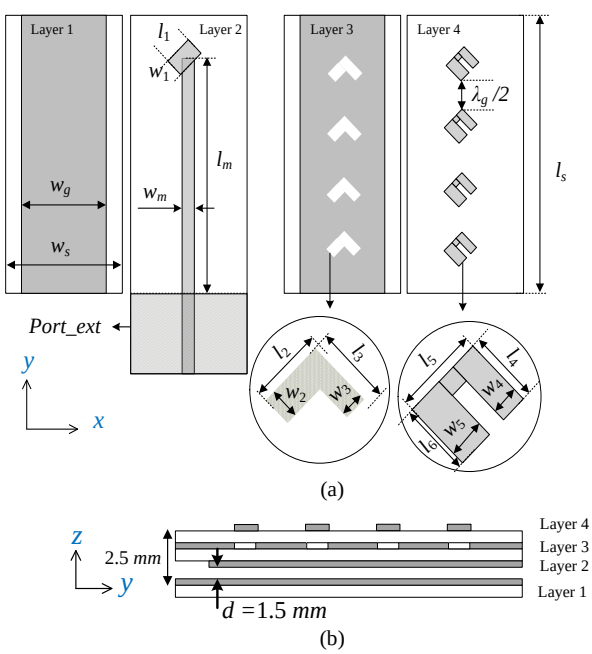

Fig. 1. Antenna geometry and layer configuration of the proposed series-fed CP antenna: (a) individual layers view, (b) side view.

The individual layers are shown in Fig. 1(a) and the side view of the layer's formation is shown in Fig. 1(b). The numerical analysis is carried out using CST Microwave Studio. The design is fully optimized before fabrication and the final optimized values are listed in Table 1.

B. Antenna Element Design and Operation Mechanism

It is well known that the polarization of the microstrip patch antenna is reliant on the lateral position of the feed. Likewise, the fundamental resonant mode of the patch with nearly square dimensions and a larger aspect ratio of more than 1.1 can degenerate [19]. For the initial sizing of the single element design, the patch dimensions are adjusted for 28 GHz. A V-shape 45-degree inclined slot with orthogonal arms was etched in the ground plane below the feedline at the half-wavelength distance from the excitation port. Along with the aperture shape, width, and length, the patch position with respect to the slot plays an important role in attaining proper excitation of the fields for circular polarization.

Each arm of the slot operates at slightly different frequencies due to unequal dimensions of the slot arms. The 45-degree inclined patch with nearly square dimensions is printed on another substrate layer for aperture coupling, and stacked on top of the slot. By properly positioning the patch edges with respect to the slot, the two edges are aligned parallel to both sides of the slot. The fundamental radiating mode is degenerated with slightly different frequency such that $f_{10} < f < f_{01}$. The resonant mode associated with the larger-size edge is slightly below, whereas the one associated with the smaller edge is above the center operating frequency of the antenna.

To widen the impedance bandwidth and the AR bandwidth, a slot is carved in the patch along the smaller edge. This creates an additional current path and enables the current to flow along the direction of the shorter edge, which degenerates the fundamental mode at a slightly higher frequency and widen the impedance bandwidth. All the dimensions of the slot and patch are simultaneously optimized at the full-wave level of description to merge the modes and to accomplish a 90-degree phase difference between the modes. To clearly illustrate the dominant field pattern with the phase progression, the surface current distribution on the patch at different angular time intervals are illustrated in Fig. 2 at 28 GHz. At zero degrees, the all the dominant field components are in the *xy*-direction and the currents along the edges add up in phase. At 90 degrees, it can be seen that the out-of-phase current along the edge in the *xy*-direction causes power cancelation, under the far-field condition, as shown with X and the dominant fields are oriented along the *yx*-direction. Similarly, for 180 degrees and 270 degrees the field orientation changes to –*xy*- and –*yx*-direction. The rotation of the field is in the anti-clockwise direction, therefore the power radiated into the space is right-hand CP. For the implementation of the half-wavelength array and to attain maximum gain in the broadside direction, the patches are placed at a $\lambda_g/2$= 2.914 mm distance. To avoid any pattern null and to ensure proper excitation of all radiating patches as well the combination of the field vectors, the series array consists only four radiators. If higher gain is desired, more elements can

MOST WIEDZY Downloaded from mostwiedzy.pl

6-1225 (c) 2020 IEEE. Personal use is permitted, but republication/redistribution requires IEEE permission. See http://www.ieee.org/publications_standards/publications/rights/index.html for more information.
Authorized licensed use limited to: Reykjavik University. Downloaded on January 19,2021 at 12:47:27 UTC from IEEE Xplore. Restrictions apply.

This article has been accepted for publication in a future issue of this journal, but has not been fully edited. Content may change prior to final publication. Citation information: DOI 10.1109/LAWP.2021.3049901, IEEE Antennas and Wireless Propagation Letters

be added. Numerical experiments indicate that incorporation of seven elements may improve the gain to 14 dBic, yet the analysis of field distribution indicates improper element excitation due to the fading effects. Furthermore, increasing the number of elements leads to enlarging the structure, i.e., a practical design requires working out the trade-off between the antenna size and the achievable gain value.

III. EXPERIMENTAL VALIDATION

A. Analysis of Return Loss and Axial Ratio

A prototype of the antenna is fabricated and characterized in free-space and on-body as shown in Fig. 3. For mounting the Southwest end-launch connector (1092-03A-6), the excitation layer in extended along the length and width, while the substrate widths of other layers are extended for mechanical alignment. To maintain the injection of exact phases to every radiator, the feed layer (Layer 2, see Fig. 1(a)) is extended by one guided wavelength along the length of the microstrip line. For characterizing the antenna, the IEEE standard test procedures (IEEE Std149-1979 (R2008)) are adopted. All the measurements are performed in the fully calibrated anechoic chamber of Reykjavik University, Iceland.

The reflection coefficient of the antenna, illustrated in Fig. 4, is well below the –10dB reference for all cases considered. The free space impedance bandwidth of the antenna shows that the antenna is operating from 27.2 GHz to 30.35 GHz.

TABLE I OPTIMIZED PARAMETER VALUES

Parameter	Value	Parameter	Value	Parameter	Value
l_1	2.7	l_4	2.37	l_s	28.7
w_1	1.81	w_4	0.862	w_s	13
l_2	3.12	l_5	2.767	w_g	10
w_2	1.1	w_m	1.05	l_m	27.14+5.828
l_3	2.85	w_3	1.327	l_6	2.427

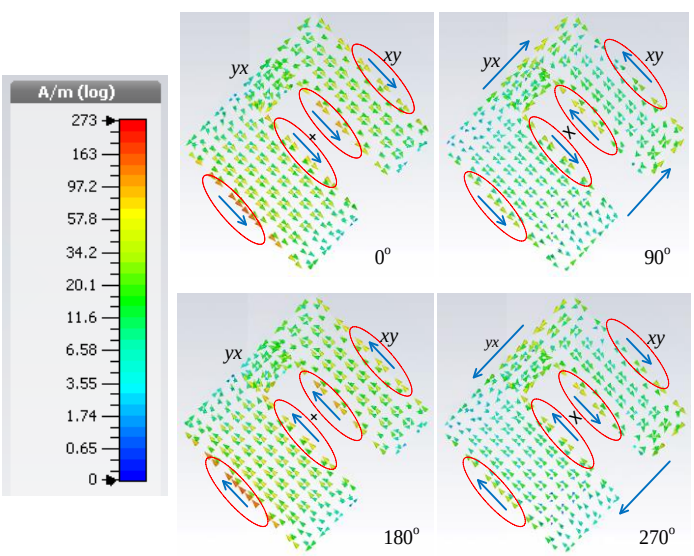

Fig. 2. Illustration of the dominant field components at different angular time intervals.

For the on-body characterization, the antenna is mounted on the human volunteer arm and chest. The clothing gap between the human body and the antenna is in the range of 2 to 3 mm. A slight improvement in the impedance matching is observed for on-body scenarios, which is due to the energy absorption by human tissues. The simulated and measured 3 dB axial ratio is shown in Fig. 5. It indicates that the CP bandwidth of the antenna is from 27.3 GHz 29.7 GHz. Although there is a small variation in the AR when the antenna is worn on-body, which could be ascribed to the presence of human and the small inadvertent movements. However, the antenna retains acceptable in-band AR characteristics in both the free space and on-body.

B. Analysis of Realized Gain and Efficiency

The simulated and measured realized gain of the antenna in free space and on-body is depicted in Fig. 6. The measured peak gain of the antenna is 11.65 dBic recorded at 28 GHz. A gain drop of roughly one dB is observed when the antenna is mounted on the chest. Overall, a stable gain is seen for both the simulated and the measured characteristics within the operating band of the antenna. The radiation efficiency (RE) and the total efficiency (TE) of the antenna are shown in Fig. 7. The RE and TE of the antenna in the free space is 90.5% and 89%, respectively. The PEC layers behind the feedline reflect all the energy in the off-side direction of the body, but a small gain drop is observed when the antenna is mounted on the body. The peak radiation efficiency of the antenna is centered at the 28.5 GHz, where all the field vectors of the radiating patches are combined. The minimum efficiency is observed near the lower cutoff frequency, where the radiation efficiency is reduced to roughly 83%.

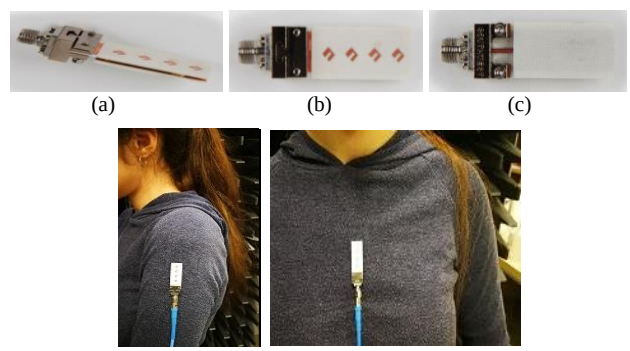

Fig. 3. Antenna prototype and characterization: (a) perspective view, (b) front view, (c) rear view, (d) antenna on-arm, (d) antenna on-chest.

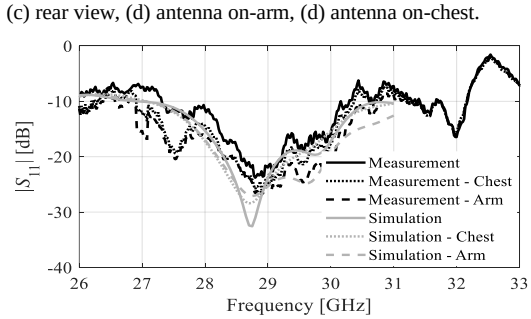

Fig. 4. Simulated (gray) and measured (black) reflection coefficient of the antenna in the free-space and on body.

MOST WIEDZY Downloaded from mostwiedzy.pl

6-1225 (c) 2020 IEEE. Personal use is permitted, but republication/redistribution requires IEEE permission. See http://www.ieee.org/publications_standards/publications/rights/index.html for more information.
Authorized licensed use limited to: Reykjavik University. Downloaded on January 19,2021 at 12:47:27 UTC from IEEE Xplore. Restrictions apply.

This article has been accepted for publication in a future issue of this journal, but has not been fully edited. Content may change prior to final publication. Citation information: DOI 10.1109/LAWP.2021.3049901, IEEE Antennas and Wireless Propagation Letters

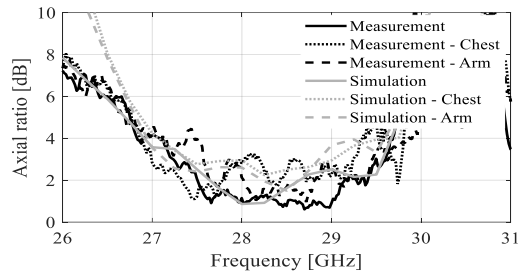

Fig. 5. Simulated (gray) and measured (black) antenna axial ratio in the free-space and on body.

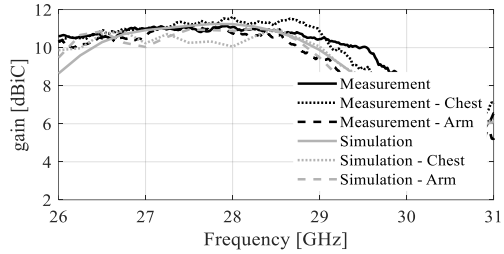

Fig. 6. Simulated (gray) and measured (black) realized gain of the antenna.

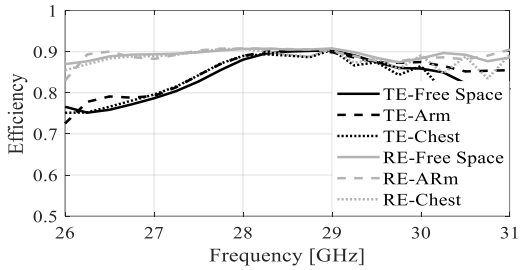

Fig. 7. Total efficiency (gray) and radiation efficiency (black) of the antenna.

C. Radiation Pattern Analysis and Benchmarking

The radiation pattern of the proposed series inclined slot antenna in the xz- and yz-plane is shown in Figs. 8. A high-gain standard horn antenna was used to measure the patterns. To make sure the antenna is operating in the directional manner, the radiation patterns are evaluated at two frequency points including 27.5 GHz, and 29 GHz. The normalized Co-polarized fields in the xz-plane shows that the antenna maintain a stable in-band directional pattern in the broadside direction. Moreover, as the antenna elements are placed in the y-direction, the yz-plane plane is of utmost importance. The cross-polarization level (left-hand CP) is well below the co-polarized (right-hand CP), which shows high polarization purity of the antenna. The slight asymmetry in the *xy*-plane is due to the unequal arms of the inclined slot. Both the simulated and the measured results in the yz-plane confirm a stable directional pattern, which is highly desirable for mm-wave applications.

A comprehensive benchmarking of the proposed antenna with recently published designs is performed by comparing multiple performance figures in Table II. For fair comparison, the bandwidths are shown in GHz because of the large difference in the operating frequencies of the antennas. It should be noted that, to date, there is a limited work published on single-port CP designs operating in the mm-wave band. The proposed antenna outperforms the reference designs in almost all aspects. Furthermore, it has the advantage of being easy-to-fabricate.

IV. Conclusion

In this letter, a circularly polarized series inclined slot-fed array is presented for Ka-band 28 GHz mm-wave applications. The antenna design comprises microstrip-line-fed aperture coupled patches. Circular polarization is realized by degenerating the fundamental mode in the nearly square patch by properly aligning the patch with the orthogonal edges of the V-shape slot. Numerical analysis and experimental validation of the antenna demonstrate that the proposed antenna features excellent performance both in the free-space and on body. As there is no official release of the permissible specific absorption rate (SAR) levels at mm-wave frequencies, the SAR analysis is not included. The primary advantages of the proposed antenna include design simplicity, high directivity, low cost, ease of fabrication, and single-point feeding.

Acknowledgment

The authors would like to thank Dassault Systemes, France, for making CST Microwave Studio available.

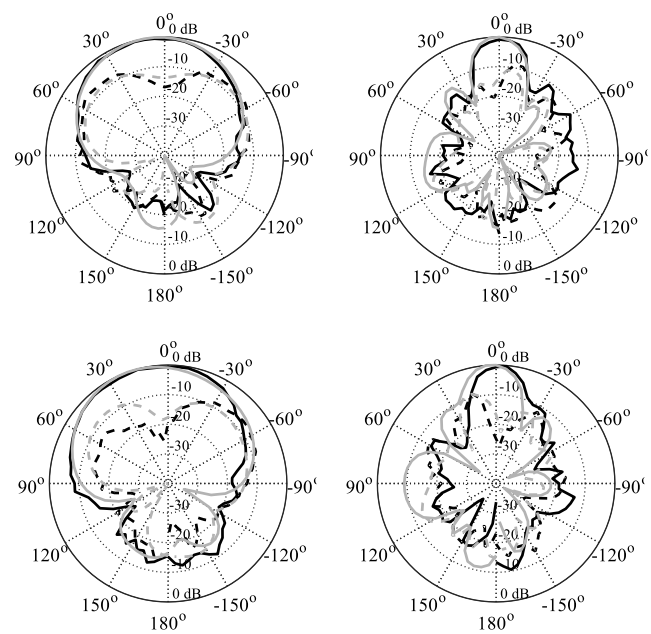

Fig. 8. Simulated (gray) and measured (black) xz- (left) and yz-plane (right) patterns for 27.5 GHz, and 29.0 GHz (from top to bottom); co-pol (—), cross-pol (- - -).

TABLE II Comparison with State-of-The-Art CP Antennas

Ref	Freq (GHz)	AR BW (GHz)	Imp BW (GHz)	Array Elements	Peak Gain (dBic)	No of Layers	On-Body Analysis
[20]	10	1	0.55	7	12	1	No
[21]	2.37	0.04	0.015	4	9.8	1	No
[22]	7.2	1	1	24	---	2	No
[23]	17	1.3	0.5	4	9.36	3	No
[24]	5.5	0.7	0.2	5	12.4	2	No
[19]	24	---	1	10	---	2	No
[20]	29	1.97	2	6	11.3	1	No
Prop	28	2.4	3.05	4	11.65	4	Yes

MOST WIEDZY Downloaded from mostwiedzy.pl

6-1225 (c) 2020 IEEE. Personal use is permitted, but republication/redistribution requires IEEE permission. See http://www.ieee.org/publications_standards/publications/rights/index.html for more information.
Authorized licensed use limited to: Reykjavik University. Downloaded on January 19,2021 at 12:47:27 UTC from IEEE Xplore. Restrictions apply.

REFERENCES

[1] W. Lin, R. W. Ziolkowski, and T. C. Baum, "28 GHz compact omnidirectional circularly polarized antenna for device-to-device communications in the future 5G systems," *IEEE Trans. Antennas Propag*., vol. 65, no. 12, pp. 6904–6914, Dec. 2017.

[2] T. S. Rappaport et al., "Millimeter wave mobile communications for 5G cellular: It will work," *IEEE Access*, vol. 1, pp. 335–349, 2013.

[3] Y. Wang, J. Li, L. Huang, Y. Jing, A. Georgakopoulos, and P. Demestichas, "5G mobile: Spectrum broadening to higher-frequency bands to support high data rates," *IEEE Veh. Technol. Mag*., vol. 9, no. 3, pp. 39–46, Sep. 2014.

[4] Z. Pi and F. Khan, "An introduction to millimeter-wave mobile broadband systems," *IEEE Commun. Mag*., vol. 49, no. 6, pp. 101–107, Jun. 2011.

[5] M. Asaadi and A. Sebak, "High-gain low-profile circularly polarized slotted SIW cavity antenna for MMW applications," *IEEE Antennas Wireless Propag. Lett.*, vol. 16, pp. 752–755, 2017.

[6] T. Deckmyn, M. Cauwe, D. Vande Ginste, H. Rogier and S. Agneessens, "Dual-Band (28,38) GHz Coupled Quarter-Mode Substrate-Integrated Waveguide Antenna Array for Next-Generation Wireless Systems," *IEEE Trans. Antennas Propag*., vol. 67, no. 4, pp. 2405-2412, April 2019.

[7] Y. Yashchyshyn *et al*., "28 GHz Switched-Beam Antenna Based on S-PIN Diodes for 5G Mobile Communications," *IEEE Antennas Wireless Propag. Lett.*, vol. 17, no. 2, pp. 225-228, Feb. 2018.

[8] U. Ullah, M. Al-Hasan, S. Koziel and I. B. Mabrouk, "Circular Polarization Diversity Implementation for Correlation Reduction in Wideband Low-Cost Multiple-Input-Multiple-Output Antenna," *IEEE Access*, vol. 8, pp. 95585-95593, 2020.

[9] U. Ullah and S. Koziel, "A Novel Coplanar-Strip-Based Excitation Technique for Design of Broadband Circularly Polarization Antennas With Wide 3 dB Axial Ratio Beamwidth," *IEEE Trans. Antennas Propag.*, vol. 67, no. 6, pp. 4224-4229, June 2019.

[10] U. Ullah, S. Koziel and I. B. Mabrouk, "Rapid Redesign and Bandwidth/Size Tradeoffs for Compact Wideband Circular Polarization Antennas Using Inverse Surrogates and Fast EM-Based Parameter Tuning," *IEEE Trans. Antennas Propag.*, vol. 68, no. 1, pp. 81-89, Jan. 2020.

[11] S. S. Hesari and J. Bornemann, "Wideband circularly polarized substrate integrated waveguide endfire antenna system with high gain," *IEEE Antennas Wireless Propag. Lett.*, vol. 16, pp. 2262–2265, 2017.

[12] H. Al-Saedi, W. M. Abdel-Wahab, S. Gigoyan, R. Mittra and S. Safavi-Naeini, "Ka-Band Antenna With High Circular Polarization Purity and Wide AR Beamwidth," *IEEE Antennas and Wireless Propagation Letters*, vol. 17, no. 9, pp. 1697-1701, Sept. 2018.

[13] H. Chen, Y. Shao, Y. Zhang, C. Zhang and Z. Zhang, "A Low-Profile Broadband Circularly Polarized mmWave Antenna With Special-Shaped Ring Slot," *IEEE Antennas Wireless Propag. Lett.*, vol. 18, no. 7, pp. 1492-1496, July 2019.

[14] S. Park and S. Park, "LHCP and RHCP Substrate Integrated Waveguide Antenna Arrays for Millimeter-Wave Applications," *IEEE Antennas Wireless Propag. Lett.*, vol. 16, pp. 601-604, 2017.

[15] Y. Lang, S. W. Qu, and J. X. Chen, "Wideband circularly polarized substrate integrated cavity-backed antenna array," *IEEE Antennas Wireless Propag. Lett.*, vol. 13, pp. 1513–1516, 2014.

[16] C. Di Paola, S. Zhang, K. Zhao, Z. Ying, T. Bolin and G. F. Pedersen, "Wideband Beam-Switchable 28 GHz Quasi-Yagi Array for Mobile Devices," *IEEE Trans. Antennas Propag.*, vol. 67, no. 11, pp. 6870-6882, Nov. 2019.

[17] Y. Cao, K.-S. Chin, W. Che, W. Yang and E. S. Li, "A compact 38 GHz multibeam antenna array with multifolded butler matrix for 5G applications", *IEEE Antennas Wireless Propag. Lett.*, vol. 16, pp. 2996-2999, 2017.

[18] F. Kuo and R. Hwang, "High-Isolation X-Band Marine Radar Antenna Design," *IEEE Trans. Antennas Propag.*, vol. 62, no. 5, pp. 2331-2337, May 2014.

[19] M. I. Aksum, S.-L. Chuang and Y. T. Lo, "On slot-coupled microstrip antennas and their application to CP operation-theory and experiment", *IEEE Trans. Antennas Propagat.*, vol. 38, pp. 1224-1230, Aug. 1990.

[20] S. J. Chen, C. Fumeaux, Y. Monnai, and W. Withayachumnankul, "Dual circularly polarized series-fed microstrip patch array with coplanar proximity coupling," *IEEE Antennas Wireless Propag. Lett.*, vol. 16, pp. 1500-1503, 2017.

[21] P. D. Hilario Re, D. Comite, and S. K. Podilchak, "Single-layer series-fed planar array with controlled aperture distribution for circularly polarized radiation," *IEEE Trans. Antennas Propagat.*, vol. 68, no. 6, pp. 4973-4978, June 2020.

[22] T. R. Cameron, A. T. Sutinjo, and M. Okoniewski, "A circularly polarized broadside radiating "herringbone" array design with the leaky-wave approach," *IEEE Antennas Wireless Propag. Lett.*, vol. 9, pp. 826-829, 2010.

[23] K. Wei, J.-Y. Li, R. Xu, and G.-W. Yang, "Circularly polarized omnidirectional microstrip antenna array," *Proc. IEEE Int. Symp. Antennas Propag.*, Jul. 2017, pp. 2315–2316.

[24] P. Hallbjörner, I. Skarin, K. From, and A. Rydberg, "Circularly polarized traveling-wave array antenna with novel microstrip patch element," *IEEE Antennas Wireless Propag. Lett.*, vol. 6, pp. 572–574, 2007.

[25] G. F. Hamberger, S. Trummer, U. Siart, and T. F. Eibert, "A planar dual-polarized microstrip 1-D-beamforming antenna array for the 24-GHz band," *IEEE Trans. Antennas Propagat.*, vol. 65, no. 1, pp. 142-149, Jan. 2017.

[26] Y. Yang, B. Sun, and J. Guo, "A low-cost, single-layer, dual circularly polarized antenna for millimeter-wave applications," *IEEE Antennas Wireless Propag. Lett.*, vol. 18, no. 4, pp. 651-655, April 2019.

MOST WIEDZY Downloaded from mostwiedzy.pl

6-1225 (c) 2020 IEEE. Personal use is permitted, but republication/redistribution requires IEEE permission. See http://www.ieee.org/publications_standards/publications/rights/index.html for more information.
Authorized licensed use limited to: Reykjavik University. Downloaded on January 19,2021 at 12:47:27 UTC from IEEE Xplore. Restrictions apply.